Tumor Detection *in vivo* with Optical Spectroscopy

V. Misic [a,d], B. A. Winey [b], H. Liu [a], L. Liao [a,c], P. Okunieff [a], K. J. Parker [d], B. Fenton [a], Y. Yu [a]

Radiation Oncology [a], Departments of Physics and Astronomy [b],
Radiology [c], and School of Engineering and Applied Science [d]
University of Rochester,
Rochester, NY 14627

Abstract: Ultrasound induced blood stasis has been observed for a long time, but to date most experimental observations have been *in vitro*. In this paper we discuss a possible diagnostic use for this previously undesirable effect of ultrasound - tumor detection *in vivo*. We demonstrate that, using optical spectroscopy, effects of ultrasound can be used to differentiate tumor from non-tumor in murine tissue. Finally, we propose a novel diagnostic algorithm that quantitatively differentiates tumor from non-tumor with maximum specificity 0.83, maximum sensitivity 0.79, and area under ROC curve 0.90.

I. INTRODUCTION

It has been well documented that stationary ultrasound waves can create bands of red blood cells *in vitro* [1]. It has been also demonstrated that even a traveling pressure wave, with small amounts of reflection at the tissue boundaries can cause banding of blood cells in the plasma medium [2]. It has been found that although the red blood cells are impeded for only short periods of time, the plasma continues to flow [3]. However, one of the limiting factors of studying this ultrasound-induced phenomenon has been the difficulty of measuring when and how much the blood actually stops during diagnostic imaging.

In separate experiments [4, 5], it has been shown that the hemoglobin oxygen saturation can be estimated from the spectroscopic measurements of light reflected from tissue.

Winey et al. [6] combined focused standing wave ultrasound induced blood stasis and optical spectroscopy, to develop a noninvasive imaging tool with potential utility in tissue diagnostics. When standing wave ultrasound is used to slow or stop the blood flow, the oxy-hemoglobin saturation decreases as the available oxygen is depleted. These changes in saturation can be monitored using the optical spectroscopy measurements, and it has been observed that saturation returns to pre-ultrasound levels shortly after the ultrasound radiation is stopped.

In this paper we demonstrate that this phenomenon can be used to aid optical spectroscopy in tumor diagnostics *in vivo*.

II. METHODS AND MATERIALS

A: Experiment Setup

The ultrasound signal used in our experiments was generated by a $\approx$ 1 MHz piezoelectric ceramic crystal mounted behind a concave aluminum lens with a focal length of 7 cm, and -6 dB focal zone. The focal zone had a diameter of 2 mm and a length of 30 mm. The signal was created by a function generator, amplified by an RF amplifier, and monitored and recorded by an oscilloscope. The ultrasonic field was measured and characterized using a hydrophone. The intensity of the ultrasound was maintained at Spatial Peak Temporal Average Intensity (SPTA) $\approx$ 0.7 mW/cm^2, averaged over the entire burst cycle.

All experiments were conducted in a water tank filled with distilled water. A sheet of aluminum was used for the acoustic reflector and a rubber block was placed behind the aluminum to absorb any scattered acoustic energy.

In order to perform non-invasive testing, a laser Doppler system was used to verify blood flow changes. Diffuse reflectance spectra were collected with a single fiber, NA = 0.22, residing at the center of a seven fiber probe. The center collection fiber was connected to a spectrometer. The outer six fibers were connected to a broadband halogen light source. The source detector separation was 1 mm, with an inspection volume of approximately 9 mm^3, mostly within 1 mm of the tissue surface. (For more details on the experiment procedures and setup, please refer to [6].)

B: Experiment Procedure

Six to eight week old C3H mice were inoculated intramuscularly to the right thigh with MCa-35 mammary carcinoma cells. The left hind leg was used as a control reference. To avoid scattering of the acoustic field, hair was removed from the hind legs. During the experiments, mice were sedated and placed in a Plexiglas restraint to position the leg away from the body. The probe was then placed on the skin of the mouse leg. Once a baseline spectrum was achieved, the mouse and probe were moved such that the focus of the ultrasound was $\approx$ 2 mm directly under the location of the optical probe. The direction of propagation of the ultrasound and light were kept orthogonal.

During each experiment, ultrasound was typically administered in 5-second bursts, with approximately 55-second relaxation periods between bursts and a total of six

bursts per leg per experimental collection. For each mouse, both legs, one with a tumor and one without, were subjected to ultrasound and optical spectroscopy to compare the response in tumor versus non-tumor tissue as part of the diagnostic portion of this experiment..

Ultrasound pulse information for each experiment was stored for later signal correlation studies. Optical spectra were sampled in 500 ms intervals. The raw optical signal was corrected for the curvature of the light source intensity. First, the spectra were cropped to regions between 475 nm and 650 nm where significant changes in optical absorption are present due to oxy/deoxy hemoglobin shifts. In that range, certain isolated wavelengths were initially considered for further study (515 nm, 528 nm, 540 nm, 560 nm, and 578 nm), but eventually the *560/540* signal ratio was chosen (the ratio of intensities at 560 nm and 540 nm).

III. ANALYSIS

By visual inspection of *560/540* and its comparison with the ultrasound signal [6], one can establish a visual temporal correlation between the two in the non-tumor scans, and the absence of such a correlation in the tumor scans (Fig. 1.). Our first experiment was designed to demonstrate that it was possible to establish the mathematical correlation between the *560/540* ratio and the ultrasound signal. The second experiment was aimed at the creation of a novel diagnostic algorithm based on a single experimental observation.

A.   Experiment I: Signal/Ultrasound Correlation
Visual correlation between the *560/540* ratio and ultrasound bursts was visually evident in most cases.
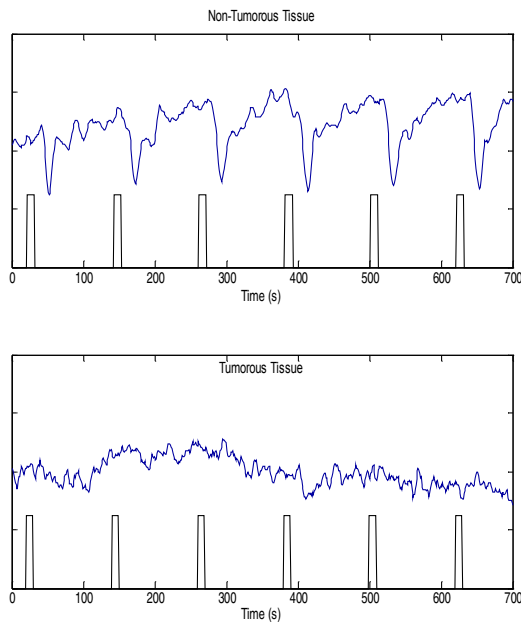

Fig. 1. The ultrasound signal in non-tumorous tissue causes more prominent "dips" in the observed *560/540* signal, than in the tumorous tissue. The measurements were not always this obvious.

The bursts of ultrasound caused pronounced drops in the observed *560/540* signals. In this experiment, we quantified that correlation and demonstrated that it is significantly different between probe readings of tumor and non-tumor tissue responses. The algorithm we used in this experiment was as follows:

1. The original ultrasound (*US*) signal was modified ("boxed") (Fig. 2.) as:

$$BUS = \begin{cases} 0 & , US\ off \\ 1 & , US\ on \end{cases} \qquad (1)$$

2. The general slope (i.e. *trend*) of the *560/540* signal was approximated using 2nd degree polynomial interpolation, and the *BUS* (1) has been scaled down and adjusted to the signal trend:

$$AUS = trend - BUS / 20 \qquad (2)$$

3. To characterize the *560/540* vs. *US* correlation, we used cross-covariance of *560/540* and *AUS*. In statistics, cross-covariance assesses the degree to which two variables co-vary or vary together. It is computed as the mean of the products of the mean deviations for each variable in the observed set. Thus, the cross-covariance between recorded *560/540* signal (*R*) and adjusted (*AUS*) ultrasound signal was calculated as cross-correlation function of two sequences with their means removed:

$$XCov(m) = E[(R(n+m)-MA) * \\ conj(AUS(n)-MAUS)] \qquad (3)$$

where *MR* and *MAUS* stand for the means of *R* and *AUS* respectively, *E* stands for the *Mathematical Expectation*, *conj* is complex-conjugate operator, and *m* and *n* are position indices in the signal.

4. The *XCov* signal was smoothed using the Savitzky-Golay (polynomial) FIR smoothing filter, with the polynomial order 3 and window size 41 [7].
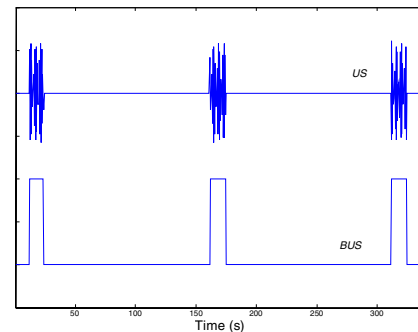

Fig. 2. Original ultrasound signal (*US*) and its "boxed" representation (*BUS*)

5. The standard deviation of the smoothed *XCov* signal was calculated.
6. Procedures described in 1-5 were performed for measurements taken on both tumor and non-tumor hind legs, and the ratio of the measurements

$$\text{Std}(XCov_{nontumor})/\text{Std}(XCov_{tumor}) \tag{4}$$

was calculated and recorded.
7. The procedures described in steps 1-6 were repeated for a total of 24 mice.

Results of this experiment are presented in Fig. 3. The ratio of the standard deviations (4) was greater than 1 (one) in all but one experiment, and greater than 2 (two) in 75% of measured mice.

B: Experiment II: Diagnostic Algorithm

Upon confirmation that there was a correlation between ultrasound bursts and observed changes ("dips") in the observed signal, we constructed a novel diagnostic algorithm that utilized that information.

1. The ultrasound (*US*) signal was modified as in (1).
2. Locations of the centers of each ultrasound burst were found and used to split *560/540* to non-overlapping "windows" bounded by those centers. The end of observation at the right side bounded the rightmost "window" (Fig. 4.).
3. The general slope (i.e. *trend*) of the *560/540* signal was approximated using 2nd degree polynomial interpolation, and the difference between *trend* and *560/540* was calculated.
4. The positions of the local minima of the difference function (calculated for each "window") were calculated.
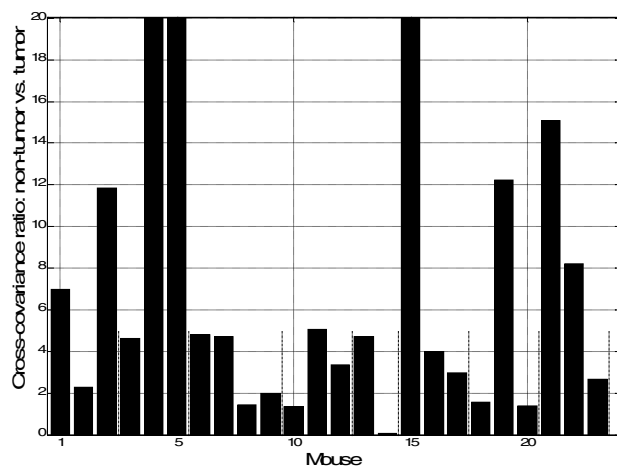

Fig. 3. The *560/540* signal in non-tumorous tissue is better correlated to the ultrasound than the same signal for tumorous tissue, measured for the same mouse to compensate for physiological differences in mice population.
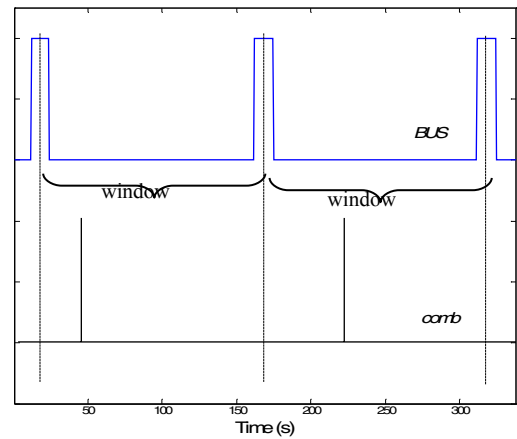

Fig. 4. Illustration of "boxed" ultrasound signal (*BUS*), observation "windows", and *comb* signal with spikes at the positions of local minima (calculated for each "window")

5. The new (*comb*) signal with ones at the position of local minimums, and zeros elsewhere was constructed (Fig. 4.).
6. The maximum of the correlation between ultrasound (*BUS*) signal and *comb* signal was calculated.
7. The ratio

$$r = (sum(comb) - max(corr)) / sum(comb) \tag{5}$$

was calculated and compared to a decision threshold *dt*.

The experiment was repeated for varying values of the decision threshold, and a Receiver-Operating Characteristics (ROC) curve was calculated. The algorithm achieved the best results with the decision threshold set to *dt* = 0.40: specificity was 83.3% and sensitivity was 79.2%. Complete results of this experiment are presented in Table 1 and Fig. 5. Experiment testbed is presented in Fig. 6.
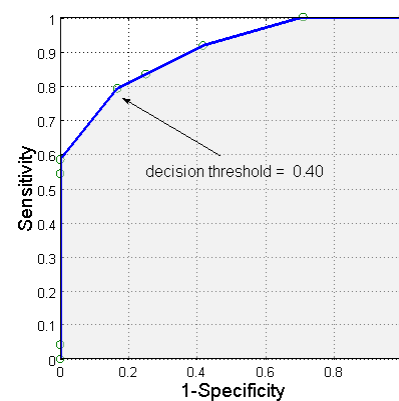

Fig. 5. ROC curve for the diagnostic algorithm. Decision threshold varied from 0.1 to 1 in 0.05 steps. Area under the curve is 0.90.
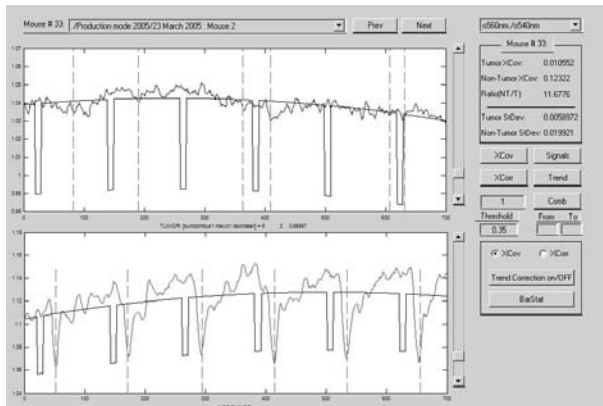
Fig. 6 Experiment Testbed: trend adjusted ultrasound (*AUS*) is superimposed over *560/540* signal. Dashed lines denote positions of local minima

IV. DISCUSSION

Results of the first experiment revealed evident differences between tumor and non-tumor measurements and demonstrated that optical spectroscopy measurements of acoustically induced blood stasis could be used to differentiate between tumor and non-tumor tissues in vivo. Variations in the experimental results (from mouse to mouse) were most likely related to variations in the experimental conditions (mouse movements, probe pressure, probe positioning, etc.).

The second experiment demonstrated that it is possible to quantitatively differentiate tumor from non-tumor based on a single non-invasive measurement. In this experiment, we first established the experimental procedure (constructed the decision-making algorithm) and then varied the value of the decision threshold in search of an optimum (the point on the curve closest to the (0,1) coordinates. It was found that for the decision threshold values of 0.40 and 0.45, the algorithm reached a specificity of 0.83 and a sensitivity of 0.79. As a measure of the algorithm accuracy, the initial assessment of the area under the ROC curve (by this experiment) was 0.90 (meaning that the constructed algorithm is indeed a very good classifier). The authors believe that, with improvements in the experimental procedure and fine-tuning of the algorithm, accuracy of the proposed classifier can be further improved.

In the future, we will investigate the cross-correlation between observed signals and various physiological properties of the tissue (vascular orientation, blood flow volume, number of blood vessels in the probed tissues, etc.) to better interpret the observed phenomenon. However, the main goal will be to mathematically quantify the signal reading versus the ultrasound correlation and to validate the automatic signal classifier as a diagnostic tool.

REFERENCES

[1] M. Dyson, B. Woodward, J.B. Pond, "The flow of red blood cells stopped by ultrasound," *Nature*, vol. 232, pp. 572-573, 1971.

[2] N.V. Baker, "Segregation and sedimentation of red blood cells in ultrasonic standing waves," *Nature*, vol. 239, pp 398-399, 1972.

[3] G. ter Haar, M. Dyson, "Effects of ultrasound on circulation," *Biorheology*, vol. 4, p 207, 1977.

[4] W.L. Nyborg, "Biological effects of ultrasound: development of safety guidelines. Part II: General Review," *Ultrasound Med. Biol.*, vol. 27, pp. 301-333, 2001.

[5] W.G. Zijlstra, A. Buursma, W.P. Meeuwsen-van der Roest, "Absorption spectra of human fetal and adult oxyhemoglobin de-oxyhemoglobin, carboxyhemoglobin and methemoglobin," *Clin. Chem.*, vol. 37, pp. 1633-1638, 1991.

[6] B.A. Winey, V. Misic, H. Liu, L. Liao, P. Okunieff, K.J. Parker, B. Fenton, Y. Yu, "*In vivo Optical Spectroscopy of Acoustically induced Blood Stasis*", submitted to EMBC 2005, Shanghai, China

[7] S.J. Orfanidis, Introduction to Signal Processing, Prentice-Hall, Englewood Cliffs, NJ, 1996.